Computers and Concrete, *Vol. 22, No. 2 (2018) 227-237*
DOI: https://doi.org/10.12989/cac.2018.22.2.227

Evaluation of constitutive relations for concrete modeling based on an incremental theory of elastic strain-hardening plasticity

Petr Král[*], Petr Hradil[a] and Jiří Kala[b]

Institute of Structural Mechanics, Faculty of Civil Engineering, Brno University of Technology, Veveří 331/95, 602 00 Brno, Czech Republic

(Received March 13, 2018, Revised July 13, 2018, Accepted July 16, 2018)

Abstract. Today, the modeling of concrete as a material within finite element simulations is predominantly done through nonlinear material models of concrete. In current sophisticated computational systems, there are a number of complex concrete material models which are based on theory of plasticity, damage mechanics, linear or nonlinear fracture mechanics or combinations of those theories. These models often include very complex constitutive relations which are suitable for the modeling of practically any continuum mechanics tasks. However, the usability of these models is very often limited by their parameters, whose values must be defined for the proper realization of appropriate constitutive relations. Determination of the material parameter values is very complicated in most material models. This is mainly due to the non-physical nature of most parameters, and also the large number of them that are frequently involved. In such cases, the designer cannot make practical use of the models without having to employ the complex inverse parameter identification process. In continuum mechanics, however, there are also constitutive relations that require the definition of a relatively small number of parameters which are predominantly of a physical nature and which describe the behavior of concrete very well within a particular task. This paper presents an example of such constitutive relations which have the potential for implementation and application in finite element systems. Specifically, constitutive relations for modeling the plane stress state of concrete are presented and subsequently tested and evaluated in this paper. The relations are based on the incremental theory of elastic strain-hardening plasticity in which a non-associated flow rule is used. The calculation result for the case of concrete under uniaxial compression is compared with the experimental data for the purpose of the validation of the constitutive relations used.

Keywords: constitutive relations; elastic strain-hardening plasticity; non-associated flow rule; concrete; yield surface; stress-strain curve

1. Introduction

Concrete is currently one of the most widely used materials in the construction industry as it offers certain advantages over other materials, one of the most distinct of which is the variety of shapes that can be formed from the material. The continuous and currently ever more extensive use of concrete in the building of new structures is leading designers and calculation specialists to work on making the designs of such structures more accurate via finite element simulations (Wu *et al*. 2015, Zhang *et al*. 2016, Moscoso *et al*. 2017). However, this effort to design safer, more durable and simultaneously far more economical concrete structures requires the involvement of nonlinear mechanics tools. With regard to the fact that the deformations occurring in concrete structures are usually very small, the involvement of nonlinear mechanics tools primarily entails the application of nonlinear material models of concrete within numerical simulations. Comprehensive modern computer programs based on the finite element method (Adina 1997, Atena 2013, ANSYS 2014, Ls-Dyna 2017) currently enable the application of a whole range of nonlinear models of concrete whose constitutive relations are mainly based on plasticity theory, damage mechanics, linear or nonlinear fracture mechanics and combinations of those theories. The realization of the constitutive relations of such models in finite element simulations depends on their parameter values, however. The determination of these values is often very difficult as the majority of models include a large quantity of parameters of a mathematical and non-physical nature. Unfortunately, when using such models, the designer or calculation specialist is thus often unable to avoid having to perform the inverse identification of material parameters, which tends to be a very complex process (Jankowiak and Łodygowski 2005, Nguyen and Korsunsky 2006). Within the continuum mechanics tasks, it is still possible to use constitutive relations which require the definition of a relatively small amount of parameters. These parameters are mainly of a physical nature and describe the behavior of real concrete very satisfactorily. Example of such constitutive relations which have the potential to be utilized via implementation in computational systems is presented below within this paper. Nevertheless, before the implementation of constitutive relations in a

*Corresponding author, Ph.D. Student
E-mail: kral.p@fce.vutbr.cz
[a]Ph.D.
E-mail: hradil.p@fce.vutbr.cz
[b]Associate Professor
E-mail: kala.j@fce.vutbr.cz

 ISSN: 1598-8198 (Print), 1598-818X (Online)

computational system it is always necessary to test and evaluate them in the context of basic tasks, which is the aim of the investigation described in this paper.

The constitutive relations employed within this paper are intended for use in modeling the plane stress state of concrete and are based on the incremental theory of elastic strain-hardening plasticity (Hu and Schnobrich 1989, Schwer and Murray 1994, Grassl and Jirasek 2006). With regard to plasticity-based models, models which described concrete as an elastic-perfectly plastic material (Kaufmann 1998, Szcześniak and Stolarski 2016) were used in the past. However, as time went on, elastic strain-hardening plastic material models proved to be more general and more suitable for the description of the real behavior of concrete than elastic-perfectly plastic material models. From the point of view of the description of the real behavior of concrete using constitutive relations, the selection of the flow rule is also important. It determines the dependence of plastic strain increments on stress increments. When modeling, there is a choice between an associated and a non-associated flow rule. It was demonstrated in the past that a non-associated flow rule is more suitable for the modeling of multi-axial stress state of concrete than an associated flow rule (Lade *et al*. 1987). With regard to the fact that also the modeling of the biaxial stress state of concrete is part of the paper, a non-associated flow rule is used for all executed calculations. Further aspects which need to be defined for the completeness of the constitutive relations used, such as yield surfaces, hardening rule, plastic hardening modulus and equivalent uniaxial stress-strain curve, are described below in the paper. These aspects are, in contrast with the work of Hu and Schnobrich (1989), modified in certain manners with regard to this paper for the purpose of obtaining better calculation results. The constitutive relations used are tested and evaluated on tasks concerning the uniaxial stress of concrete in compression and tension and the biaxial stress of concrete in compression while placing emphasis on the evaluation of both the pre-peak and post-peak behavior of concrete. For the purpose of the validation of constitutive relations, the result for the uniaxial compression of concrete is compared with experimental data.

2. Theoretical background of constitutive relations

2.1 Yield surfaces

Within this paper, constitutive relations are based on the incremental theory of elastic strain-hardening plasticity. It is typical for strain-hardening models that after the achievement of an initial yield surface, subsequent yield surfaces change in relation to continued plastic straining up to the moment of the achievement of the ultimate yield surface (see Fig. 1). Moreover, all yield surfaces can be described by the same yield function within the theory of plasticity. For the modeling of concrete, the yield function can be divided further into a total of three yield functions, each of which can be used for the description of one of the three regions of the yield surface (the tension-tension region, the compression-tension region and the compression-compression region). In this paper, yield functions were used which were defined separately for each of the previously mentioned regions of biaxial tension (tension-tension region), compression-tension and biaxial compression (compression-compression region) (Hand *et al*. 1972, Hu and Schnobrich 1989). The corresponding yield surfaces are shown in Fig. 1.

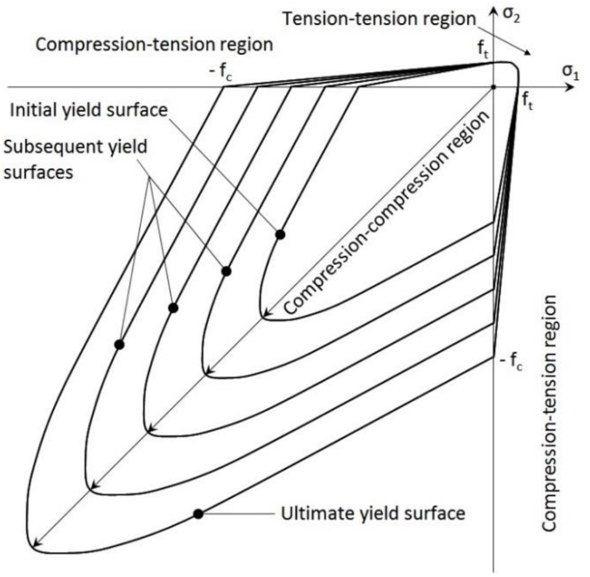

Fig. 1 Yield surfaces of concrete in the principal stress plane

As far as the tension-tension region is concerned, it can be seen from Fig. 1 that only linearly elastic concrete behavior without the occurrence of plastic deformation is assumed from the beginning of load up to the failure of the material. This is because the initial yield surface is identical to the ultimate yield surface (failure surface). The yield function for the tension-tension region is expressed in the following mathematical form

$$f\left(\{\boldsymbol{\sigma}\}^{\mathrm{T}}\right)=F\left(\{\boldsymbol{\sigma}\}^{\mathrm{T}}\right)-f_c=c_1\left(\frac{3}{2\sqrt{2}}\frac{1+\alpha}{\alpha}\tau_{oct}+\right.$$
$$\left.+\frac{3}{2}\frac{1-\alpha}{\alpha}\sigma_m\right)-f_c=0 \tag{1}$$

where $\{\boldsymbol{\sigma}\}^{\mathrm{T}}=\{\sigma_x, \sigma_y, \tau_{xy}\}$ is the row stress vector for plane stress, f_c is the maximum uniaxial compressive strength of concrete, and the variable α depends on parameters f_c and f_t according to the equation

$$\alpha=\frac{f_t}{f_c} \tag{2}$$

where f_t is the maximum uniaxial tensile strength of concrete. In Eq. (1), σ_m is the mean stress, which is defined as follows for the case of plane stress

$$\sigma_m=\frac{1}{3}\left(\sigma_x+\sigma_y\right) \tag{3}$$

and τ_{oct} is the octahedral shear stress, defined as

$$\tau_{oct}=\frac{\sqrt{2}}{3}\sqrt{\sigma_x^2-\sigma_x\sigma_y+\sigma_y^2+3\tau_{xy}^2} \tag{4}$$

The parameter c_1 can be expressed by the following equation:

$$c_1 = 1 - 0.4019\left(\frac{\sigma_2}{\sigma_1}\right) + 0.008913\left(\frac{\sigma_2}{\sigma_1}\right)^2 \tag{5}$$

where σ_1 and σ_2 are principal stresses for which it is true that $\sigma_1 \geq \sigma_2$ (both principal stresses have positive values).

In the case of the compression-tension region where concrete is exposed to compressive and tensile strain simultaneously, the yield function can be expressed using the following equation:

$$f\left(\{\boldsymbol{\sigma}\}^{\mathrm{T}}, \sigma_{eqv}\right) = F\left(\{\boldsymbol{\sigma}\}^{\mathrm{T}}\right) - \sigma_{eqv} = c_2\left(\frac{3}{2\sqrt{2}}\frac{1+\alpha}{\alpha}\tau_{oct} + \frac{3}{2}\frac{1-\alpha}{\alpha}\sigma_m\right) - \sigma_{eqv} = 0 \tag{6}$$

where σ_{eqv} is the equivalent stress. The equivalent stress is a hardening parameter which depends on the previous stress-strain history of the material and its strain-hardening properties. As soon as the value of loading function F in Eq. (6) equals the value σ_{eqv}, yielding will occur and the equivalent stress gains a new value at the same time. The parameter c_2 can be expressed by the following equations

$$c_2 = 1 - 0.02886\left(\frac{\sigma_2}{\sigma_1}\right) - 0.006657\left(\frac{\sigma_2}{\sigma_1}\right)^2 - 0.0002443\left(\frac{\sigma_2}{\sigma_1}\right)^3 \quad \text{for} -\infty < \frac{\sigma_1}{\sigma_2} < -0.103 \tag{7}$$

$$c_2 = 1 + 6.339\left(\frac{\sigma_1}{\sigma_2}\right) + 68.82\left(\frac{\sigma_1}{\sigma_2}\right)^2 + 183.8\left(\frac{\sigma_1}{\sigma_2}\right)^3 \quad \text{for} -0.103 \leq \frac{\sigma_1}{\sigma_2} < 0 \tag{8}$$

where σ_1 is the maximum principal stress with a positive value and σ_2 is the minimum principal stress with a negative value.

In the case of the compression-compression region, where concrete is exposed only to compressive strain, the yield function is defined with the expression

$$f\left(\{\boldsymbol{\sigma}\}^{\mathrm{T}}, \sigma_{eqv}\right) = F\left(\{\boldsymbol{\sigma}\}^{\mathrm{T}}\right) - \sigma_{eqv} = c_3\left(\frac{3}{\sqrt{2}}\frac{2\beta-1}{\beta}\tau_{oct} + 3\frac{\beta-1}{\beta}\sigma_m\right) - \sigma_{eqv} = 0 \tag{9}$$

in which $\beta = 1.16$ and the parameter c_3 is defined as

$$c_3 = 1 + 0.05848\left(\frac{\sigma_1}{\sigma_2}\right) - 0.05848\left(\frac{\sigma_1}{\sigma_2}\right)^2 \tag{10}$$

where both principal stresses σ_1 and σ_2 have negative values and it is valid that $\sigma_1 \geq \sigma_2$. In this paper, in contrast with the work of Hu and Schnobrich (1989), the ratio of principal stresses in Eq. (10) is modified.

In all the given c parameters, principal stresses are defined with equations (Meyers and Chawla 2009)

$$\sigma_1 = \sigma_{max} = \frac{\sigma_x + \sigma_y}{2} + \frac{1}{2}\sqrt{\left(\sigma_x - \sigma_y\right)^2 + 4\tau_{xy}^2} \tag{11}$$

$$\sigma_2 = \sigma_{min} = \frac{\sigma_x + \sigma_y}{2} - \frac{1}{2}\sqrt{\left(\sigma_x - \sigma_y\right)^2 + 4\tau_{xy}^2} \tag{12}$$

2.2 Hardening rule and flow rule

In the case of strain-hardening models, shifts of yield surfaces occur during loading that causes plastic straining. The way in which yield surfaces are shifted is governed by a hardening rule. Various hardening rules can be applied as needed, such as kinematic hardening, isotropic hardening, and also some mixed hardening rules (Shames and Cozzarelli 1997, Rouainia and Muir Wood 2000, Rezaiee-Pajand and Nasirai 2007, Kazaz 2011). A kinematic hardening rule is suitable for modeling cyclically loaded materials in which the “Bauschinger effect” needs to be monitored. With such materials, shifts of yield surfaces do not occur during plastic deformation via their expansion, but via their distortion. For the modeling of monotonically loaded materials it is completely sufficient to use an isotropic hardening rule, with which the distortion of yield surfaces does not occur, but only their expansion. Mixed hardening rules need to be used in cases when properties such as the isotropic hardening rule and kinematic hardening rule are important for the modeling. As only monotonic loading of concrete was considered in the calculations performed for this paper, the isotropic hardening rule was used for these purposes.

With regard to the flow rule, either an associated flow rule or a non-associated flow rule (Bland 1957, Runesson and Mroz 1989) can be used within the context of the theory of plasticity. The difference between both rules consists in the type of plastic potential function involved, which is related to plastic strains. Within the framework of the associated flow rule it is assumed that the plastic potential function is equal to the yield function of the material, while in the case of the non-associated flow rule it is assumed that the plastic potential function and yield function of the material differ from each other. In this paper a non-associated flow rule was used. It can be formulated as

$$\mathrm{d}\{\boldsymbol{\varepsilon}\}_p^{\mathrm{T}} = \lambda\frac{\partial g\left(\{\boldsymbol{\sigma}\}^{\mathrm{T}}, \sigma_{eqv}\right)}{\partial\{\boldsymbol{\sigma}\}^{\mathrm{T}}} = \lambda\frac{\partial G\left(\{\boldsymbol{\sigma}\}^{\mathrm{T}}\right)}{\partial\{\boldsymbol{\sigma}\}^{\mathrm{T}}} \tag{13}$$

where λ is a positive scalar factor which can vary during the hardening process. Eq. (13) shows the relationship between the plastic potential function and the incremental plastic strain vector. In the case of elasto-plastic material models this combine with the incremental elastic strain vector to form the incremental total strain vector according to the equation

$$\mathrm{d}\{\boldsymbol{\varepsilon}\}^{\mathrm{T}} = \mathrm{d}\{\boldsymbol{\varepsilon}\}_e^{\mathrm{T}} + \mathrm{d}\{\boldsymbol{\varepsilon}\}_p^{\mathrm{T}} \tag{14}$$

where all vectors are row vectors. In non-incremental form, Eq. (14) can be written as the following equation:

$$\{\boldsymbol{\varepsilon}\}^{\mathrm{T}} = \{\boldsymbol{\varepsilon}\}_e^{\mathrm{T}} + \{\boldsymbol{\varepsilon}\}_p^{\mathrm{T}} \tag{15}$$

The plastic potential function used for calculations in this paper was as follows

$$g\left(\{\boldsymbol{\sigma}\}^{\mathrm{T}}, \sigma_{eqv}\right) = G\left(\{\boldsymbol{\sigma}\}^{\mathrm{T}}\right) - \sigma_{eqv} = \frac{3}{\sqrt{2}}\tau_{oct} - \sigma_{eqv} = 0 \tag{16}$$

2.3 Equivalent uniaxial stress-strain curve

An important aspect which needs to be defined for models including plastic strains with hardening is the equivalent uniaxial stress-strain curve in compression, to which the results of all of the different loading cases are related. For the purposes of this paper, the equivalent uniaxial stress-strain curve was used. It is defined using the mutual dependence of two parameters to which the multidimensional stress and strain conditions are related (Hu and Schnobrich 1988). This is the dependence of parameter σ_{eqv} (the equivalent stress) on parameter ε_{eqv} (the equivalent strain), which can be expressed via the following equation

$$\sigma_{eqv}=\frac{E_{c,init}\varepsilon_{eqv}}{\left[\begin{array}{l}1+\left(R+R_E-2\right)\left(\frac{\varepsilon_{eqv}}{\varepsilon^*}\right)-\left(2R-1\right)\left(\frac{\varepsilon_{eqv}}{\varepsilon^*}\right)^2+\\+R\left(\frac{\varepsilon_{eqv}}{\varepsilon^*}\right)^3\end{array}\right]} \tag{17}$$

in which the parameter $E_{c,init}$ is the initial elastic modulus and R is the ratio relation defined as

$$R=\frac{R_E\left(R_\sigma-1\right)}{\left(R_\varepsilon-1\right)^2}-\frac{1}{R_\varepsilon} \tag{18}$$

In Eqs. (17)-(18), R_E is the modular ratio, R_σ is the stress ratio and R_ε is the strain ratio. These three ratios are given by the following expressions

$$R_E=\frac{E_{c,init}}{E_{sc}} \tag{19}$$

$$R_\sigma=\frac{f_c}{\sigma_f} \tag{20}$$

$$R_\varepsilon=\frac{\varepsilon_f}{\varepsilon^*} \tag{21}$$

where ε_f is the maximum strain on the equivalent uniaxial stress-strain curve, σ_f is the stress corresponding to ε_f on the equivalent uniaxial stress-strain curve and E_{sc} is the secant modulus defined as

$$E_{sc}=\frac{f_c}{\varepsilon^*} \tag{22}$$

In Eqs. (17), (21) and (22), the parameter ε^* is the strain corresponding to f_c on the equivalent uniaxial stress-strain curve. The mathematical expression of this strain is as follows

$$\varepsilon^*=q\varepsilon_c \tag{23}$$

where ε_c is the strain corresponding to f_c within the uniaxial compression test and q is a parameter via which greater generality can be achieved for the equivalent uniaxial stress-strain curve. The parameter q depends on the type of the yield surface region which corresponds to the given stress state. If the stress state corresponds to the compression-tension region, parameter q is defined using the following equations.

For $-\infty<\sigma_1/\sigma_2<-0.103$

$$q=\frac{f_c}{E_{c,init}\varepsilon_c}+\left(1-\frac{f_c}{E_{c,init}\varepsilon_c}\right)\left[\begin{array}{l}0.001231\left(\frac{\sigma_2}{\sigma_1}\right)+\\+0.001469\left(\frac{\sigma_2}{\sigma_1}\right)^2+0.0000134\left(\frac{\sigma_2}{\sigma_1}\right)^3\end{array}\right] \tag{24}$$

and for $-0.103\leq\sigma_1/\sigma_2<0$

$$q=\frac{f_c}{E_{c,init}\varepsilon_c}+\left(1-\frac{f_c}{E_{c,init}\varepsilon_c}\right)\left[\begin{array}{l}1+13.96\left(\frac{\sigma_1}{\sigma_2}\right)+\\+59.21\left(\frac{\sigma_1}{\sigma_2}\right)^2+69.24\left(\frac{\sigma_1}{\sigma_2}\right)^3\end{array}\right] \tag{25}$$

where σ_1 is the maximum principal stress with a positive value and σ_2 is the minimum principal stress with a negative value. For the case of biaxial compression (compression-compression region), the parameter q is defined as

$$q=\frac{f_c}{E_{c,init}\varepsilon_c}+\left(1+\frac{f_c}{E_{c,init}\varepsilon_c}\right)\left[\begin{array}{l}1+1.782\left(\frac{\sigma_1}{\sigma_2}\right)+\\+0.5936\left(\frac{\sigma_1}{\sigma_2}\right)^2\end{array}\right] \tag{26}$$

where both principal stresses σ_1 and σ_2 have negative values, and it is valid that $\sigma_1\geq\sigma_2$. In calculations performed within this paper, the equivalent strain ε_{eqv} given in Eq. (17) was calculated via the following equation

$$\varepsilon_{eqv}=\frac{2}{3}\sqrt{\varepsilon_x^2-\varepsilon_x\varepsilon_y+\varepsilon_y^2+\frac{3}{4}\gamma_{xy}^2} \tag{27}$$

in which the individual strains are components of the total strain vector given for plane stress in row form as

$$\{\boldsymbol{\varepsilon}\}^{\mathrm{T}}=\{\varepsilon_x,\varepsilon_y,\gamma_{xy}\} \tag{28}$$

2.4 Plastic hardening modulus

Another important aspect which needs to be defined for models including plastic strains with hardening and which is related to the equivalent uniaxial stress-strain curve is the plastic hardening modulus. Generally, the plastic hardening modulus H_p is defined as a derivation of the function describing the shape of the equivalent uniaxial stress-strain curve according to the plastic component of the equivalent strain. This can be mathematically expressed as

$$H_p=\frac{\mathrm{d}\sigma_{eqv}}{\mathrm{d}\varepsilon_{eqv,p}} \tag{29}$$

With regard to the presence of the incremental plastic component of the equivalent strain in Eq. (29), it is clear that just as in the case of the total strain vector from Eq. (15) it is possible to divide the equivalent strain ε_{eqv} into two parts in the form of its elastic component $\varepsilon_{eqv,e}$ and plastic component $\varepsilon_{eqv,p}$. This fact can be written in incremental form as

$$\mathrm{d}\varepsilon_{eqv}=\mathrm{d}\varepsilon_{eqv,e}+\mathrm{d}\varepsilon_{eqv,p} \tag{30}$$

After dividing Eq. (30) by the incremental equivalent stress $\mathrm{d}\sigma_{eqv}$ this equation will have the form

$$\frac{\mathrm{d}\varepsilon_{eqv}}{\mathrm{d}\sigma_{eqv}}=\frac{\mathrm{d}\varepsilon_{eqv,e}}{\mathrm{d}\sigma_{eqv}}+\frac{\mathrm{d}\varepsilon_{eqv,p}}{\mathrm{d}\sigma_{eqv}}=\frac{1}{E_{c,init}}+\frac{1}{H_p}=\frac{1}{E_{tg}} \tag{31}$$

where E_{tg} is the equivalent uniaxial tangent modulus. On the basis of Eq. (31), it is now easy to obtain the specific expression needed for the calculation of the plastic hardening modulus in the form

$$H_p=\frac{E_{c,init}E_{tg}}{E_{c,init}-E_{tg}} \tag{32}$$

The mathematical expression for the equivalent uniaxial tangent modulus given in Eqs. (31)-(32) can be written as follows

$$E_{tg}=\frac{\mathrm{d}\sigma_{eqv}}{\mathrm{d}\varepsilon_{eqv}}=$$
$$=\frac{E_{c,init}\left[1+(2R-1)\left(\frac{\varepsilon_{eqv}}{\varepsilon^*}\right)^2-2R\left(\frac{\varepsilon_{eqv}}{\varepsilon^*}\right)^3\right]}{\left[\begin{array}{l}1+(R+R_E-2)\left(\frac{\varepsilon_{eqv}}{\varepsilon^*}\right)-(2R-1)\left(\frac{\varepsilon_{eqv}}{\varepsilon^*}\right)^2+\\+R\left(\frac{\varepsilon_{eqv}}{\varepsilon^*}\right)^3\end{array}\right]^2} \tag{33}$$

The shape of the equivalent uniaxial stress-strain curve, and thus the slope (sign) of the equivalent uniaxial tangent modulus, is strongly dependent on parameters ε_f and σ_f. In Hu and Schnobrich (1989) the parameters mentioned are selected in such a way that R_ε=4 and R_σ=4. Murray *et al*. (1979) also used the ratios R_ε and R_σ that were equal to 4. A disadvantage of such selected parameter values is that in the region of the equivalent uniaxial stress-strain curve after exceeding the value f_c the equivalent uniaxial tangent modulus gains negative values. This could cause considerable numerical difficulties. Within this paper, values of parameters ε_f and σ_f were not selected for all cases in such a way that ratios R_ε and R_σ equal one specific number, but they were selected so that they ensure a permanently growing equivalent uniaxial stress-strain curve for various cases in combination with other parameter values while achieving acceptable calculation results. This made use of the fact that the equivalent uniaxial stress-strain curve does not have to have the same shape as the simulated stress-strain curve for the uniaxial compression test. During the calculations, this approach provided permanently positive values for the equivalent uniaxial tangent modulus. As a result, it can be stated that it is suitable for use in the removal of the above-mentioned numerical difficulties.

2.5 The incremental form of constitutive equations

If aspects such as yield surfaces, hardening rule, flow rule, equivalent uniaxial stress-strain curve and plastic hardening modulus are defined, constitutive relations can be composed (Hu and Schnobrich 1989). Within the framework of theory of elasticity, constitutive equations can be written in the form of the generalized Hooke's law. When considering the decomposition of the total strain vector into its elastic and plastic components, the generalized Hooke's law can be written down in the incremental form in the following way

$$\mathrm{d}\{\boldsymbol{\sigma}\}=[\mathbf{C}]_e\mathrm{d}\{\boldsymbol{\varepsilon}\}_e=[\mathbf{C}]_e\left(\mathrm{d}\{\boldsymbol{\varepsilon}\}-\mathrm{d}\{\boldsymbol{\varepsilon}\}_p\right) \tag{34}$$

where $\mathrm{d}\{\boldsymbol{\sigma}\}$ is the incremental stress vector in column form and $[\mathbf{C}]_e$ is the elastic material property matrix for plane stress. The incremental form of the yield function obtained by its differentiation is given as follows

$$\begin{aligned}&\mathrm{d}f\left(\{\boldsymbol{\sigma}\}^{\mathrm{T}},\sigma_{eqv}\right)=\frac{\partial f\left(\{\boldsymbol{\sigma}\}^{\mathrm{T}},\sigma_{eqv}\right)}{\partial\{\boldsymbol{\sigma}\}^{\mathrm{T}}}\mathrm{d}\{\boldsymbol{\sigma}\}+\\&+\frac{\partial f\left(\{\boldsymbol{\sigma}\}^{\mathrm{T}},\sigma_{eqv}\right)}{\partial\sigma_{eqv}}\frac{\mathrm{d}\sigma_{eqv}}{\mathrm{d}\varepsilon_{eqv,p}}\mathrm{d}\varepsilon_{eqv,p}=0\end{aligned} \tag{35}$$

If Eqs. (13), (29) and (34) and equation

$$\frac{\partial f\left(\{\boldsymbol{\sigma}\}^{\mathrm{T}},\sigma_{eqv}\right)}{\partial\{\boldsymbol{\sigma}\}^{\mathrm{T}}}=\frac{\partial F\left(\{\boldsymbol{\sigma}\}^{\mathrm{T}}\right)}{\partial\{\boldsymbol{\sigma}\}^{\mathrm{T}}} \tag{36}$$

are applied to Eq. (35), and if it is considered that

$$\frac{\partial f\left(\{\boldsymbol{\sigma}\}^{\mathrm{T}},\sigma_{eqv}\right)}{\partial\sigma_{eqv}}=-1 \tag{37}$$

then Eq. (35) gains the following form

$$\frac{\partial F\left(\{\boldsymbol{\sigma}\}^{\mathrm{T}}\right)}{\partial\{\boldsymbol{\sigma}\}^{\mathrm{T}}}[\mathbf{C}]_e\left(\mathrm{d}\{\boldsymbol{\varepsilon}\}-\lambda\frac{\partial G\left(\{\boldsymbol{\sigma}\}^{\mathrm{T}}\right)}{\partial\{\boldsymbol{\sigma}\}}\right)-H_p\mathrm{d}\varepsilon_{eqv,p}=0 \tag{38}$$

By expressing the incremental equivalent plastic strain from the equation for the calculation of plastic work performed during plastic deformation and by applying Eq. (13), we obtain equation

$$\mathrm{d}\varepsilon_{eqv,p}=\frac{\{\boldsymbol{\sigma}\}^{\mathrm{T}}\mathrm{d}\{\boldsymbol{\varepsilon}\}_p}{\sigma_{eqv}}=\frac{\{\boldsymbol{\sigma}\}^{\mathrm{T}}\lambda\frac{\partial G\left(\{\boldsymbol{\sigma}\}^{\mathrm{T}}\right)}{\partial\{\boldsymbol{\sigma}\}}}{\sigma_{eqv}}=\lambda\frac{G\left(\{\boldsymbol{\sigma}\}^{\mathrm{T}}\right)}{\sigma_{eqv}} \tag{39}$$

By applying Eq. (39) to Eq. (38) and subsequent adjustment, an equation can be obtained for the calculation of parameter λ in the form

$$\lambda=\frac{\frac{\partial F\left(\{\boldsymbol{\sigma}\}^{\mathrm{T}}\right)}{\partial\{\boldsymbol{\sigma}\}^{\mathrm{T}}}[\mathbf{C}]_e\mathrm{d}\{\boldsymbol{\varepsilon}\}}{H_p\frac{G\left(\{\boldsymbol{\sigma}\}^{\mathrm{T}}\right)}{\sigma_{eqv}}+\frac{\partial F\left(\{\boldsymbol{\sigma}\}^{\mathrm{T}}\right)}{\partial\{\boldsymbol{\sigma}\}^{\mathrm{T}}}[\mathbf{C}]_e\frac{\partial G\left(\{\boldsymbol{\sigma}\}^{\mathrm{T}}\right)}{\partial\{\boldsymbol{\sigma}\}}} \tag{40}$$

Now, if Eq. (13) and subsequently also Eq. (40) are applied to Eq. (34), Eq. (34) gains the form

$$\begin{aligned}&\mathrm{d}\{\boldsymbol{\sigma}\}=[\mathbf{C}]_e\mathrm{d}\{\boldsymbol{\varepsilon}\}-[\mathbf{C}]_e\lambda\frac{\partial G\left(\{\boldsymbol{\sigma}\}^{\mathrm{T}}\right)}{\partial\{\boldsymbol{\sigma}\}}=\\&=[\mathbf{C}]_e\mathrm{d}\{\boldsymbol{\varepsilon}\}-[\mathbf{C}]_p\mathrm{d}\{\boldsymbol{\varepsilon}\}=\left([\mathbf{C}]_e-[\mathbf{C}]_p\right)\mathrm{d}\{\boldsymbol{\varepsilon}\}\end{aligned} \tag{41}$$

where the elastic material property matrix $[\mathbf{C}]_e$ is given as follows

Table 1 Input parameters of the user function for concrete with a uniaxial compressive strength of 33 MPa

Lab.	Loading	$E_{c,init}$ [MPa]	ν [-]	f_c [MPa]	f_t [MPa]	ε_c [-]	ε_f [-]	σ_f [MPa]	n	$1000\Delta\varepsilon_x$ [-]	$1000\Delta\varepsilon_y$ [-]	$1000\Delta\gamma_{xy}$ [-]
1	uxc	14500	0.2	33	3	0.0021	0.0035	38.5	400	-0.010	0.0020	0
2	bxc	14500	0.2	33	3	0.0021	0.0035	38.5	442	-0.010	-0.0010	0
3	bxc	14500	0.2	33	3	0.0021	0.0035	38.5	508	-0.010	-0.0030	0
4	bxc	14500	0.2	33	3	0.0021	0.0035	38.5	552	-0.010	-0.0050	0
5	bxc	14500	0.2	33	3	0.0021	0.0035	38.5	570	-0.010	-0.0070	0
6	bxc	14500	0.2	33	3	0.0021	0.0035	38.5	560	-0.010	-0.0085	0
7	bxc	14500	0.2	33	3	0.0021	0.0035	38.5	740	-0.010	-0.0100	0
8	uxt	14500	0.2	33	3	0.0021	0.0035	38.5	207	0.001	-0.0002	0

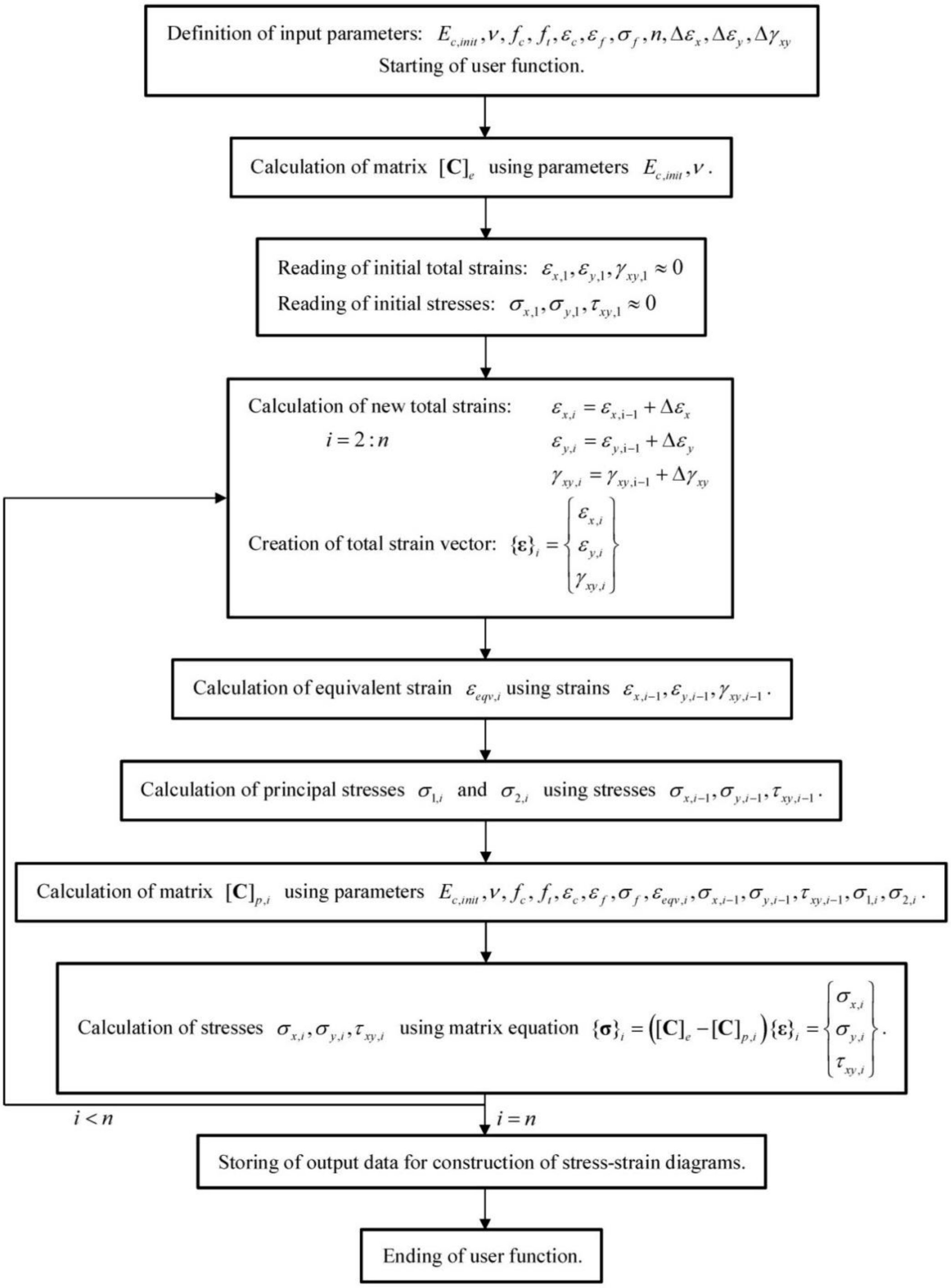

Fig. 2 Scheme of the user function algorithm

$$[\mathbf{C}]_e = \frac{E_{c,init}}{1-\nu^2}\begin{bmatrix} 1 & \nu & 0 \\ \nu & 1 & 0 \\ 0 & 0 & (1-\nu)/2 \end{bmatrix} \tag{42}$$

and where $[\mathbf{C}]_p$ is the unsymmetric plastic material property matrix defined as

$$[\mathbf{C}]_p = \frac{[\mathbf{C}]_e \dfrac{\partial G\left(\{\boldsymbol{\sigma}\}^{\mathrm{T}}\right)}{\partial\{\boldsymbol{\sigma}\}} \dfrac{\partial F\left(\{\boldsymbol{\sigma}\}^{\mathrm{T}}\right)}{\partial\{\boldsymbol{\sigma}\}^{\mathrm{T}}}[\mathbf{C}]_e}{H_p \dfrac{G\left(\{\boldsymbol{\sigma}\}^{\mathrm{T}}\right)}{\sigma_{eqv}} + \dfrac{\partial F\left(\{\boldsymbol{\sigma}\}^{\mathrm{T}}\right)}{\partial\{\boldsymbol{\sigma}\}^{\mathrm{T}}}[\mathbf{C}]_e \dfrac{\partial G\left(\{\boldsymbol{\sigma}\}^{\mathrm{T}}\right)}{\partial\{\boldsymbol{\sigma}\}}} \tag{43}$$

The parameter ν in Eq. (42) is the Poisson's ratio of concrete. The constitutive relations given in the incremental form in Eq. (41) were used for all calculations performed within this paper.

3. Calculation results and their evaluation

For this paper, all calculations were carried out using the user function which was programmed in Matlab software (Matlab 2005) and which included the constitutive equations described in the previous chapter. A simplified scheme of the algorithm of the user function is shown in Fig. 2. It can be seen from the diagram in Fig. 2 that the purpose of the user function was to simulate the plane stress state of concrete under constantly growing strain on the basis of defined input parameters. It can also be seen from Fig. 2 that the output of the user function was data which enabled the subsequent construction of stress-strain diagrams which described the behavior of plain concrete during plane stress.

Constitutive relations (material model) were tested via the user function and evaluated in a total of two cases. In the first case, they were tested for one specific type of concrete (concrete with a maximum uniaxial compressive strength of 33 MPa) via the following types of stresses: uniaxial compression (*uxc*), biaxial compression (*bxc*), uniaxial tension (*uxt*), see Table 1. In the second case, they were tested for concretes with various maximum uniaxial compressive strengths via the following types of stresses: uniaxial compression (*uxc*), uniaxial tension (*uxt*), see Table 2.

Table 1 presents the input parameters of the user function used to simulate the behavior of concrete with a maximum uniaxial compressive strength of 33 MPa for the given types of stresses (*uxc*, *bxc* and *uxt*). Parameter $\Delta\gamma_{xy}$ was defined with a zero value in all cases because shear stress τ_{xy} does not occur during the application of the above types of stresses, and as a consequence, shear strain γ_{xy} does not occur either. With regard to this fact it is clear that the normal stresses and strains in the simulated plane were equal to the principal stresses and strains. In order to maintain the generality of notation, the following equalities were selected between the stresses and strains

$$\sigma_x = \sigma_1 \tag{44}$$

$$\sigma_y = \sigma_2 \tag{45}$$

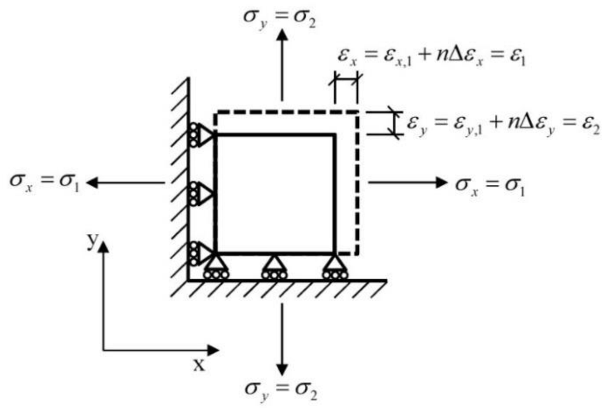

Fig. 3 Simulated plane stress state of concrete

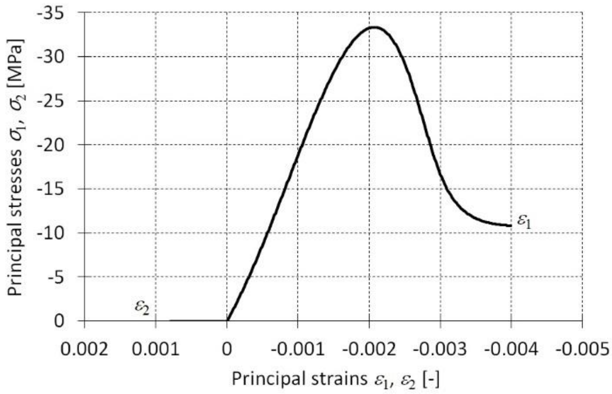

Fig. 4 Simulated stress-strain diagram for concrete under uniaxial compression (lab. 1 in Table 1)

$$\varepsilon_x = \varepsilon_1 \tag{46}$$

$$\varepsilon_y = \varepsilon_2 \tag{47}$$

With regard to the stated facts, the testing of the plane stress state of concrete executed within this paper can be depicted schematically as the plane compressive or tensile loading of a concrete element in the shape of hexahedron whose dimensions are considerably greater in the tested plane than its thickness (see Fig. 3).

Figs. 4-10 show the results of the calculations for cases 1-7 from Table 1. The results take the form of stress-strain diagrams which describe the behavior of concrete during uniaxial and biaxial compression. The axes of the stress-strain diagrams are formed by principal quantities as a result of Eqs. (44)-(47) and Fig. 3. With regard to the uniaxial compression of concrete, it can be seen from Fig. 4 that during constantly growing strain the material model displayed elasto-plastic concrete behavior with strain-hardening before attaining the maximum uniaxial compressive strength f_c with subsequent compressive strain-softening. Fig. 4 also shows that the peak of the stress-strain curve corresponds to f_c and ε_c in Table 1 completely correctly. Last but not least, Fig. 4 shows that the drop in stress caused by compressive strain-softening in the material model under further strain settled at approximately 11 MPa, which can be labeled the residual compressive strength of the concrete.

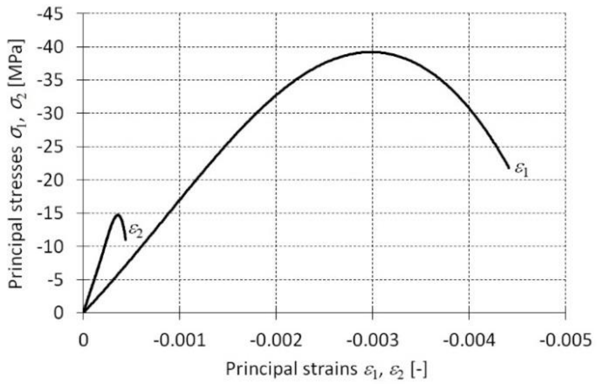

Fig. 5 Simulated stress-strain diagram for concrete under biaxial compression (lab. 2 in Table 1)

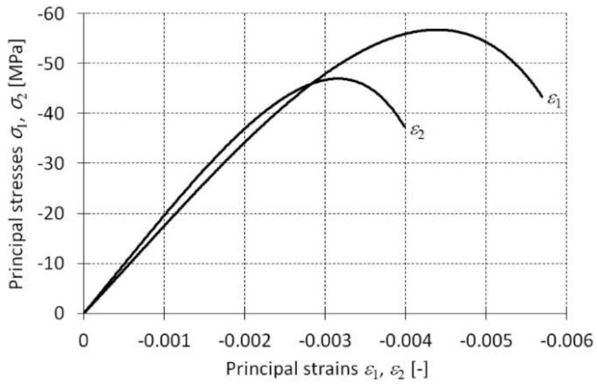

Fig. 8 Simulated stress-strain diagram for concrete under biaxial compression (lab. 5 in Table 1)

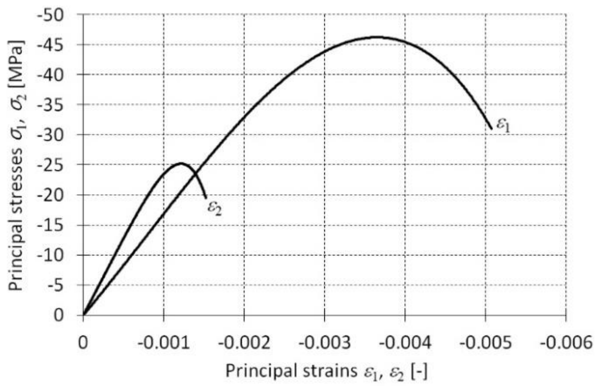

Fig. 6 Simulated stress-strain diagram for concrete under biaxial compression (lab. 3 in Table 1)

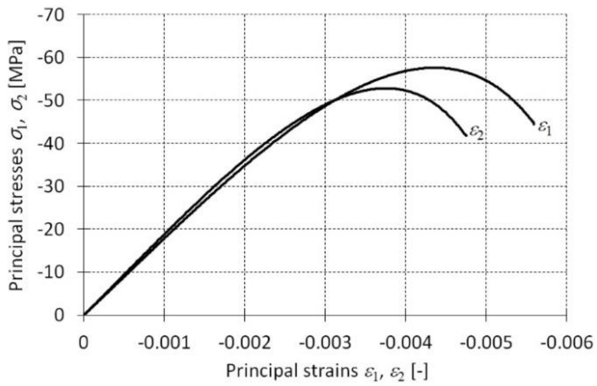

Fig. 9 Simulated stress-strain diagram for concrete under biaxial compression (lab. 6 in Table 1)

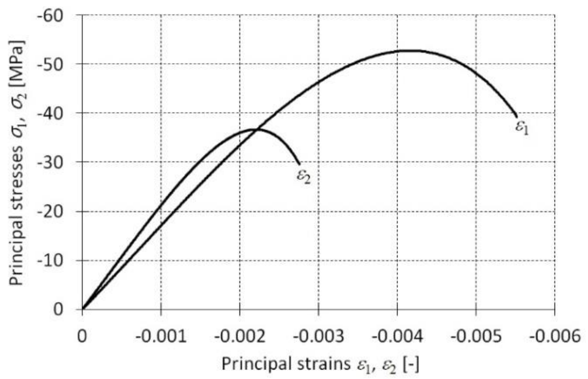

Fig. 7 Simulated stress-strain diagram for concrete under biaxial compression (lab. 4 in Table 1)

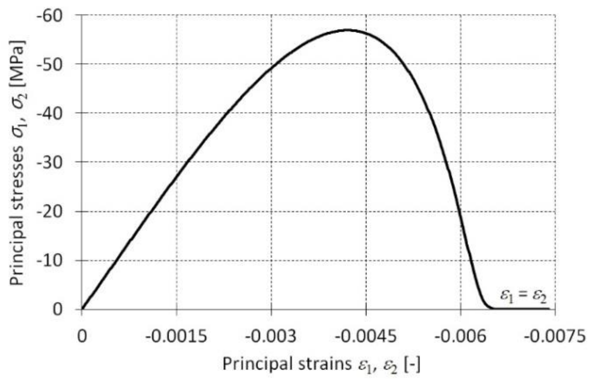

Fig. 10 Simulated stress-strain diagram for concrete under biaxial compression (lab. 7 in Table 1)

With regard to the biaxial compression of concrete, Figs. 5-10 show that during constantly growing biaxial strain the material model displayed very similar concrete behavior to that which occurs in the case of uniaxial compression. However, the peak of the stress-strain curve for the biaxial compression of concrete is shifted in comparison to the peak of the stress-strain curve for the uniaxial compression of concrete in all the simulated cases. This shows that the material model is able to simulate the growth of the maximum compressive strength and corresponding strain as a result of biaxial compressive loading. The stress state of concrete under biaxial compression is thus completely in accordance with the yield surfaces in Fig. 1.

Fig. 11 shows all simulated stress-strain curves for concrete under compression (labs. 1-7 in Table 1) and experimental data for the uniaxial compression of concrete obtained from an experimental investigation performed by Kupfer and Gerstle (1973). The purpose of Fig. 11 is both an illustrative demonstration of how the maximum compressive strength of concrete and corresponding strain both grow within the material model during increasing biaxial compressive loading and a validation of the relevant simulated data (lab. 1, *uxc*) using experimental data. The

Table 2 Input parameters of the user function for different types of concrete

Lab.	Loading	$E_{c,init}$ [MPa]	ν [-]	f_c [MPa]	f_t [MPa]	ε_c [-]	ε_f [-]	σ_f [MPa]	n	$1000\Delta\varepsilon_x$ [-]	$1000\Delta\varepsilon_y$ [-]	$1000\Delta\gamma_{xy}$ [-]
1	uxc	11700	0.2	24	2.2	0.00190	0.0035	27.2	380	-0.010	0.0020	0
2	uxc	14500	0.2	33	3.0	0.00210	0.0035	38.5	400	-0.010	0.0020	0
3	uxc	17600	0.2	43	3.9	0.00225	0.0035	50.5	420	-0.010	0.0020	0
4	uxc	20300	0.2	53	4.8	0.00240	0.0035	63.0	440	-0.010	0.0020	0
5	uxt	11700	0.2	24	2.2	0.00190	0.0035	27.2	189	0.001	-0.0002	0
6	uxt	14500	0.2	33	3.0	0.00210	0.0035	38.5	207	0.001	-0.0002	0
7	uxt	17600	0.2	43	3.9	0.00225	0.0035	50.5	222	0.001	-0.0002	0
8	uxt	20300	0.2	53	4.8	0.00240	0.0035	63.0	237	0.001	-0.0002	0

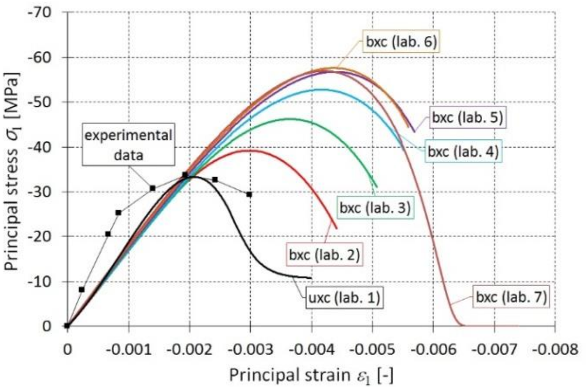

Fig. 11 Simulated stress-strain curves for the compression of concrete and experimental data

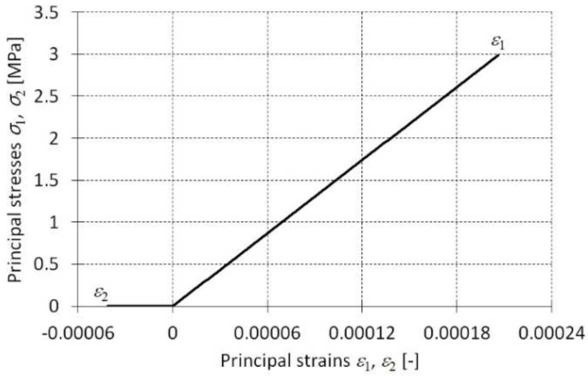

Fig. 12 Simulated stress-strain diagram for concrete under uniaxial tension (lab. 8 in Table 1)

experimental stress-strain curve in Fig. 11 corresponds to the results of a uniaxial compression test performed on a plain concrete element with the dimensions 200 mm × 200 mm × 50 mm. The comparison of the experimental curve with the simulated curve for the uniaxial compression of concrete shows that for the selected combination of input parameter values the material model is capable of accurately reproducing both the peak of the real stress-strain curve and also its shape to a certain degree. Smaller differences between both curves could be achieved by another combination of the input parameter values. However, it needs to be pointed out that for the selected combination of input parameter values, the equivalent uniaxial tangent modulus calculated within the framework of the algorithm of constitutive relations gained permanently positive values despite the fact that during compressive strain-softening the tangent modulus of the simulated stress-strain curve gained negative values, which were supposed to be achieved. An advantage of the permanently positive equivalent uniaxial tangent modulus values during the calculation could be the removal of the numerical difficulties which are usually associated with negative equivalent uniaxial tangent modulus values.

Fig. 12 shows a stress-strain diagram obtained from the calculation within which the uniaxial stretching of concrete was simulated (lab. 8 in Table 1). It can be seen from Fig. 12 that the material model displayed only linearly-elastic concrete behavior during constantly growing tensile strain up to the moment when the maximum uniaxial tensile strength f_t was achieved. This is completely in accordance with the yield surface in Fig. 1, which unambiguously specifies that no plastic deformations occur in the tension-tension region. As is shown in Fig. 12, the calculation for the uniaxial tension of concrete was terminated at the moment of the achievement of uniaxial tensile strength f_t. This was due to the fact that the constitutive relations used within this paper do not include any model via which it would be possible to capture the effect of tensile strain-softening as a result of the opening of cracks in concrete after the achievement of tensile strength f_t.

Table 2 shows the input parameters of the user function used for the simulations of the behavior of different types of concrete with various maximum uniaxial compressive strengths for the given types of stresses (*uxc* and *uxt*). The results of the computer simulations are shown in Fig. 13 for the uniaxial compression of concrete, or in Fig. 14 for the uniaxial tension of concrete. According to ACI Committee 363 (1984), growth in the maximum uniaxial compressive strength of real concrete is in particular responsible for growth in compressive strain during which compressive strength is achieved, followed by growth in the stiffness of concrete (elastic modulus of concrete). In contrast, the ductility of real concrete in compression decreases with the growth of compressive strength. Fig. 13 and Table 2 show that the material model is able to accurately reproduce the above-mentioned aspects concerning the strength and stiffness of real concrete in compression on the basis of parameters $E_{c,init}$, f_c and ε_c. With regard to the ductility of concrete in compression, Fig. 13 shows that during calculations the material model exhibited lower ductility or a steeper and more marked drop in stress with increasing compressive strength of concrete during compressive strain-

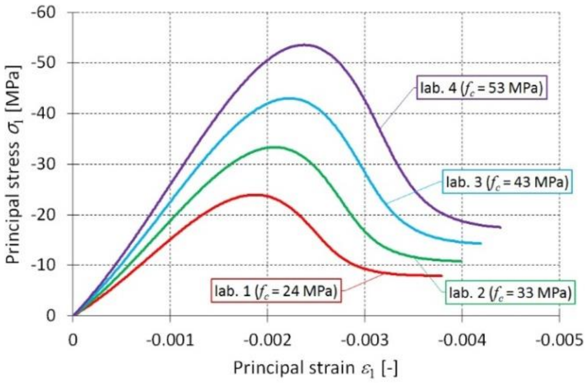

Fig. 13 Simulated stress-strain curves for different types of concrete under uniaxial compression (*uxc*)

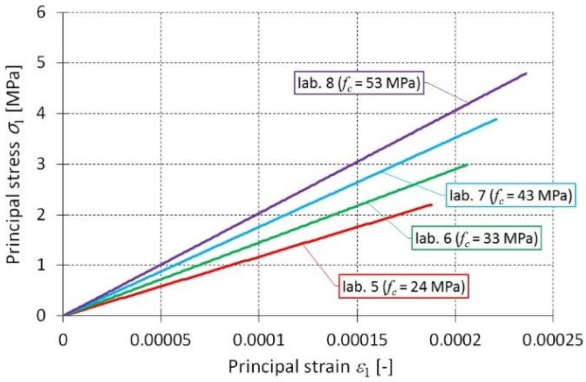

Fig. 14 Simulated stress-strain curves for different types of concrete under uniaxial tension (*uxt*)

softening. Lower ductility of concrete in compression was achieved in the calculations by increasing the value of parameter σ_f while keeping parameter ε_f at a constant value. The growth in the compressive strength of concrete seen within the calculations was (understandably) associated with the growth in the maximum uniaxial tensile strength of concrete and corresponding tensile strain, which is demonstrated in Fig. 14.

Based on the obtained calculation results and their comparison with experimental data and findings from the real testing of concrete it can be stated that the constitutive relations described and tested within this paper are a suitable tool for modeling of the behavior of real concrete in the plane stress state.

4. Conclusions

This paper described and subsequently detailed the testing and evaluation of constitutive relations (material model) which are intended for modeling the plane stress state of concrete and are based on the incremental theory of elastic strain-hardening plasticity, within the context of which the following were applied: various yield surfaces, an isotropic hardening rule, a non-associated flow rule and the equivalent uniaxial stress-strain curve. The testing of the constitutive relations was carried out via the user function programmed in Matlab software and involved basic tasks such as the uniaxial compression and tensile testing of different types of concrete and the biaxial compression testing of concrete with a maximum uniaxial compressive strength of 33 MPa. The result of the calculation (stress-strain curve) performed for the uniaxial compression of concrete with a maximum uniaxial compressive strength of 33 MPa was compared with appropriate experimental data (a real stress-strain curve). The comparison showed that for the used combination of input parameter values the tested material model is able to accurately reproduce both the peak of the real stress-strain curve and, to a certain degree, also its shape. The used combination of input parameter values also resulted in permanently positive values being gained by the equivalent uniaxial tangent modulus calculated within the algorithm of constitutive relations. This fact could be used advantageously in the removal of numerical difficulties which are usually connected with negative equivalent uniaxial tangent modulus values. Based on the executed calculations and comparisons, the conclusion can be drawn that the constitutive relations used have the potential to be used successfully within finite element computational systems as they appear to be a suitable tool for modeling the behavior of real concrete in a plane stress state.

Acknowledgments

This paper was created with the financial support of project GACR 17-23578S "Damage assessment identification for reinforced concrete subjected to extreme loading" provided by the Czech Science Foundation.

References

ACI Committee 363 (1984), "State of the art report on high-strength concrete", *ACI Journal*, **81**(4), 364-411.
ADINA (1997), *ADINA: Theory and Modeling Guide*, ADINA R&D Inc.
ANSYS (2014), *ANSYS Mechanical Theory Reference Release 15.0*, ANSYS Inc.
ATENA (2013), *ATENA Program Documentation*, Cervenka consulting Ltd., Prague, Czech Republic.
Bland, D. R. (1957), "The associated flow rule of plasticity", *Journal of the Mechanics and Physics of Solids*, **6**(1), 71-78.
Grassl, P. and Jirasek, M. (2006), "Damage-plastic model for concrete failure", *International Journal of Solids and Structures*, **43**(22-23), 7166-7196.
Hand, F. R., Pecknold, D. A. and Schnobrich, W. C. (1972), "A layered finite element nonlinear analysis of reinforced concrete plates and shells", Civil Engineering Studies, Structural Research Series No. 389, University of Illinois at Urbana-Champaign, Urbana-Champaign, Illinois.
Hu, H.-T. and Schnobrich, W. C. (1989), "Constitutive modeling of concrete by using nonassociated plasticity", *Journal of Materials in Civil Engineering*, **1**(4), 199-216.
Hu, H.-T. and Schnobrich, W. C. (1988), "Nonlinear analysis of plane stress state reinforced concrete under short term monotonic loading", Civil Engineering Studies, Structural Research Series No. 539, University of Illinois at Urbana-Champaign, Urbana-Champaign, Illinois.

Jankowiak, T. and Łodygowski, T. (2005), "Identification of parameters of concrete damage plasticity constitutive model", *Foundations of Civil and Environmental Engineering*, **6**, 53-69.

Kaufmann, W. (1998), *Strength and Deformations of Structural Concrete Subjected to In-Plane Shear and Normal Forces*, Springer Basel AG, Zurich, Switzerland.

Kazaz, I. (2011), "Finite element analysis of shear-critical reinforced concrete walls", *Computers and Concrete*, **8**(2), 143-162.

Kupfer, H. and Gerstle, K. (1973), "Behaviour of concrete under biaxial stress", *Journal of the Engineering Mechanics Division*, ASCE, **99**, 852-866.

Lade, P. V., Nelson, R. B. and Ito, Y. M. (1987), "Nonassociated flow and stability of granular materials", *Journal of Engineering Mechanics*, ASCE, **113**(9), 1302-1318.

LS-Dyna (2017), *Theory Manual*, Livemore Software Technology Corporation, Livemore, California, USA.

Matlab (2005), *The Language of Technical Computing*, The MathWorks, Inc.

Meyers, M. A. and Chawla, K. K. (2009), *Mechanical Behavior of Materials*, Cambridge University Press, New York, NY, USA.

Moscoso, A. M., Tamayo, J. L. P. and Morsch, I. B. (2017), "Numerical simulation of external pre-stressed steel-concrete composite beams", *Computers and Concrete*, **19**(2), 191-201.

Murray, D. W., Wong, C., Rijub-Agha, K. Y. and Chitnuyanondh, L. (1979), "Concrete plasticity theory for biaxial stress analysis", *Journal of the Engineering Mechanics Division*, ASCE, **105**(6), 989-1006.

Nguyen, G. D. and Korsunsky, A. M. (2006), "Damage-plasticity modelling of concrete: Calibration of parameters using separation of fracture energy", *International Journal of Fracture*, **139**(2), 325-332.

Rezaiee-Pajand, M. and Nasirai, C. (2007), "Accurate integration scheme for von-Mises plasticity with mixed-hardening based on exponential maps", *Engineering Computations*, **24**(6), 608-635.

Rouainia, M. and Muir wood, D. (2000), "A kinematic hardening constitutive model for natural clays with loss of structure", *Géotechnique*, **50**(2), 153-164.

Runesson, K. and Mroz, Z. (1989), "A note on nonassociated plastic flow rules", *International Journal of Plasticity*, **5**(6), 639-658.

Schwer, L. E. and Murray, Y. D. (1994), "A three invariant smooth cap model with mixed hardening", *International Journal for Numerical and Analytical Methods in Geomechanics*, **18**, 657-688.

Shames, I. H. and Cozzarelli, F. A. (1997), *Elastic and Inelastic Stress Analysis*, CRC Press, Taylor & Francis Group, Boca Raton, Florida, USA.

Szcześniak, A. and Stolarski, A. (2016), "A simplified model of concrete for analysis of reinforced concrete elements", *Bulletin of the Military University of Technology*, **65**(4), 55-68.

Wu, M., Chen, Z. and Zhang, C. (2015), "Determining the impact behavior of concrete beams through experimental testing and meso-scale simulation: I. Drop-weight tests", *Engineering Fracture Mechanics*, **135**, 94-112.

Zhang, D., Wang, Q. and Dong, J. (2016), "Simulation study on CFRP strengthened reinforced concrete beam under four-point bending", *Computers and Concrete*, **17**(3), 407-421.

CC